A Cross-Band Quantum Light Source Based on Spontaneous Four-Wave Mixing in a Shallow-Ridge Silicon Waveguide

Yijia Wang(王艺佳)[1], Qirui Ren(任启锐)[1], Zhanping Jin(金展平)[1], Yidong Huang(黄翊东)[1,2], and Wei Zhang(张巍)[1,2*]

[1]*State Key Laboratory of Low Dimensional Quantum Physics, Frontier Science Center for Quantum Information, Department of Electronic Engineering, Tsinghua University, Beijing 100084, China*
[2]*Beijing Academy of Quantum Information Sciences, Beijing 100193, China*

(Received 30 July 2025; accepted manuscript online 24 November 2025)

To fully utilize the resources provided by optical fiber networks, a cross-band quantum light source generating photon pairs, where one photon in a pair is at C band and the other is at O band, is proposed in this work. This source is based on spontaneous four-wave mixing (SFWM) in a piece of shallow-ridge silicon waveguide. Theoretical analysis shows that the waveguide dispersion could be tailored by adjusting the ridge width, enabling broadband photon pair generation by SFWM across C band and O band. The spontaneous Raman scattering (SpRS) in silicon waveguides is also investigated experimentally. It shows that there are two regions in the spectrum of generated photons from SpRS, which could be used to achieve cross-band photon pair generation. A chip of shallow-ridge silicon waveguide samples with different ridge widths has been fabricated, through which cross-band photon pair generation is demonstrated experimentally. The experimental results show that the source can be achieved using dispersion-optimized shallow-ridge silicon waveguides. This cross-band quantum light source provides a way to develop new fiber-based quantum communication functions utilizing both C band and O band and extends applications of quantum networks.

DOI: 10.1088/0256-307X/43/1/010601 CSTR: 32039.14.0256-307X.43.1.010601

Quantum entanglements are important resources for quantum communication and quantum information processing. The quantum light sources for telecom-band entangled photon pair generation are crucial in various quantum communication applications over optical fibers, such as quantum key distribution,[1–7] entanglement swapping,[8,9], quantum teleportation,[10] and so on. The commonly used transmission bands in optical fibers are the conventional band (C band) near 1550 nm and the original band (O band) near 1310 nm. The photons at C band have the lowest transmission loss in silica single-mode fibers. Usually, C-band entangled photon pairs are preferred to achieve long entanglement distribution distances. Both spontaneous down conversion (SPDC) and spontaneous four-wave mixing (SFWM) can be used to generate C-band entangled photon pairs. In SPDC, a pump photon is annihilated, generating a signal photon and an idler photon simultaneously. To satisfy energy conservation in the process, a pump light near 800 nm is required to generate C-band photon pairs in periodically poled second-order nonlinear crystals, such as periodically poled Lithium Niobate (PPLN).[11–13] In some works, the pump light is generated by an intense laser at 1.5 μm through second harmonic generation in the periodically poled crystals.[14] Recently, it has been achieved using PPLN waveguides, showing its potential for applications of quantum photonic chips.[15,16] In SFWM, two pump photons are annihilated, generating a signal photon and an idler photon simultaneously. The pump light is also at C band, stimulating SFWM in third-order nonlinear waveguides such as optical fibers and silicon waveguides, which are widely used in optical fiber communication and optical integration.[17–19] Hence, it provides a convenient way to realize C-band quantum light sources using mature materials and commercial components.[20,21] At present, quantum light sources at C band have been widely used in quantum communications over optical fiber networks.[22,23] On the other hand, the O band is near the zero-dispersion point of commonly used single-mode fibers; hence, the impact of fiber dispersion would be highly reduced for photons at this band. Besides, InP/InGaAsP single-photon avalanche photodiodes used at near-infrared bands have much better performance at O band than that at C band. Hence, O band is also an attractive choice for quantum communications over optical fibers. Fiber-based SFWM sources have been achieved to generate photon pairs at O band and have been applied in quantum communication experiments over optical fibers.[24]

To fully utilize the resources provided by optical fiber networks, a quantum light source generating photon pairs, where one photon in a pair is at C band and the other is at O band, is helpful for developing new network functions using the two bands. For example, it can be used in scenarios where entanglement distribution should be im-

*Corresponding author. Email: zwe@tsinghua.edu.cn

plemented from the source to two users through two fiber links, but only the C band of one fiber link is available while that of the other link is occupied by classical optical communication signals. It can also be used to teleport the quantum state of a photon at one band, e.g., C band, to a photon at another band, e.g., O band. However, it is not easy to generate such cross-band photon pairs through SPDC and SFWM. In principle, this source can be realized by SPDC in a carefully designed periodically poled crystal. But precise temperature control is required since the quasi-phase matching condition of SPDC is highly sensitive to the poling period. SFWM in silica optical fibers requires a fiber length of several hundred meters due to its low nonlinearity, limiting the bandwidth of generated photon pairs. Broadband noise photons generated by spontaneous Raman scattering (SpRS) in fibers are also a limitation in this application.[25] Silicon waveguides with lengths of several millimeters can support photon pair generation through SFWM thanks to their high third-order nonlinearity. However, the large waveguide dispersion of commonly used single-mode strip waveguides limits the bandwidth of photon pair generation. It can be expected that dispersion engineering could be applied to extend the bandwidth of SFWM; however, dispersion-engineered waveguides such as width-modulated silicon waveguides[26–28] and silicon slot waveguides[29,30] always have complex structures and are not easy to fabricate. The phase matching between different transverse modes of waveguides can also achieve efficient nonlinear interactions over broad bandwidths; this has been successfully demonstrated for generating octave-spanning frequency combs and correlated photon pairs.[31,32] However, the difficulty in coupling light into or out of specific transverse modes within a waveguide remains an issue that cannot be ignored. Besides, the impact of SpRS in silicon waveguides on this application remains unclear. So far, such a cross-band source has not been achieved based on SFWM.

In this work, we propose and demonstrate that this cross-band source can be achieved by SFWM in a piece of shallow-ridge silicon waveguide. By properly designing the width of the ridge, the zero dispersion point of the waveguide can be optimized to ∼1420 nm, which is the selected pump wavelength of SFWM for broadband photon pair generation in this source. The impact of SpRS in silicon waveguides is also investigated experimentally, showing that it does not seriously influence the quality of photon pair generation in two frequency shift regions. Finally, the cross-band source generating photon pairs, where one photon in a pair is at C band and the other is at O band, is demonstrated using shallow-ridge silicon waveguides and commercial fiber components, showing its potential for applications requiring both bands in optical fiber networks.

To show the principle and feasibility of the proposed cross-band quantum light source, the spectra of photon flux intensity generated by SFWM in silicon waveguides are calculated under a continuous wave (CW) pump light near 1420 nm. The calculation consists of two steps. First, the propagation coefficients and mode field areas of the waveguide at different wavelengths from 1300 nm to 1565 nm are calculated using the Finite-Difference Eigenmode (FDE) solver (Lumerical MODE). Then, the photon flux intensity spectra of SFWM in the waveguide are calculated according to the following equation:

$$f = \frac{(\gamma PL)^2}{2\pi}\mathrm{sinc}^2\Big(\frac{\Delta\beta L}{2}\Big), \tag{1}$$

where P is the pump power, L is the length of the silicon waveguide, and $\Delta\beta$ represents the phase mismatch. $\Delta\beta$ can be calculated by

$$\Delta\beta = \beta(\lambda_{\mathrm{s}}) + \beta(\lambda_{\mathrm{i}}) - 2\beta(\lambda_{\mathrm{p}}) + 2\gamma P, \tag{2}$$

where $\beta(\cdot)$ is the propagation coefficient under the wavelengths of the pump light (λ_{p}), signal photons (λ_{s}), and idler photons (λ_{i}), respectively. These wavelengths satisfy the energy conservation condition of SFWM, i.e., $\frac{2}{\lambda_{\mathrm{p}}} = \frac{1}{\lambda_{\mathrm{s}}} + \frac{1}{\lambda_{\mathrm{i}}}$. γ is the nonlinear coefficient of the waveguide, calculated as

$$\gamma = \frac{2\pi n_2}{\lambda A_{\mathrm{eff}}}, \tag{3}$$

where n_2 denotes the nonlinear refractive index of silicon, approximately $n_2 = 0.45 \times 10^{-13}\,\mathrm{cm}^2/\mathrm{W}$. A_{eff} is the effective mode field area of the silicon waveguide, which can be simulated using the FDE solver.

First, the calculation results of a single-mode strip waveguide are shown in Fig. 1. This type of silicon waveguide is widely used in quantum light sources at C band. The sketch of its cross-section is shown in Fig. 1(a). The height and width of its silicon core are 220 nm and 450 nm, respectively. Previous works have shown that the photon flux intensity generated by SFWM in the quasi-TE mode is far higher than that in the quasi-TM mode;[33] hence, only the quasi-TE mode is considered in the following calculation. The calculated waveguide dispersions of the quasi-TE mode are shown in Fig. 1(b). In the figure, D (ps/nm/km) is a parameter describing the waveguide dispersion, which is defined as $D = -\frac{2\pi c}{\lambda^2}\beta_2$, where β_2 is the group velocity dispersion of the waveguide mode. It can be seen that the quasi-TE mode has large anomalous dispersion ($D > 0$) over a broad wavelength region. Then, the photon flux intensity spectra of SFWM under different waveguide widths are calculated under the condition that the waveguide length is set to 8 mm, with a pump wavelength set to 1420 nm and a pump power set to 10 mW. The results are shown in Fig. 1(c). The y-axis of the figure quantifies spectral intensity by spectral density of photon flux, which describes generated photon number per nanosecond within a spectral bandwidth of 1 THz. It can be seen that a wider spectral width could be expected under a narrower waveguide width. However, none of them can cover both O band and C band. Figure 1(d) shows the calculated spectral density of photon flux of SFWM under different waveguide lengths, with the condition that the waveguide width is set to 450 nm, the pump wavelength is set to 1420 nm, and the pump power is set to 10 mW. The light blue and green regions indicate O band and C band respectively. It can be seen that the maximum photon flux intensity rises when the waveguide length increases,

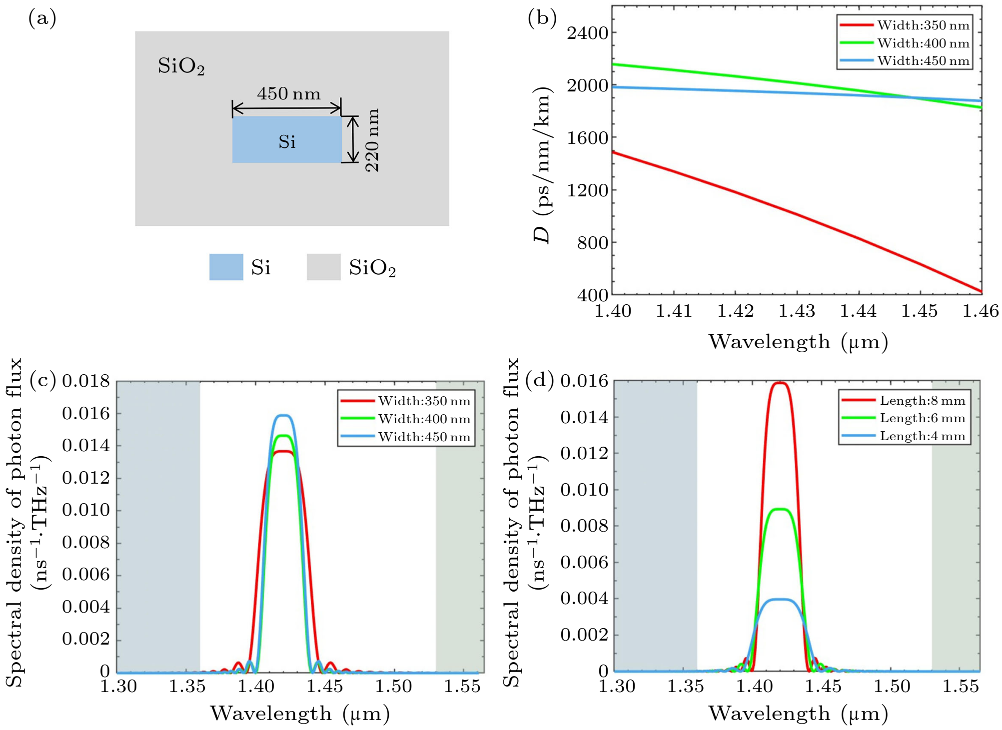

Fig. 1. Calculation results of a single-mode strip silicon waveguide with a cross-sectional size of 450 nm × 220 nm. (a) The sketch of the silicon waveguide cross-section. (b) Dispersion curves of the quasi-TE mode of the waveguides with different widths. (c) Photon flux intensity spectra of SFWM in the quasi-TE mode under different waveguide widths. The pump wavelength is set to 1420 nm, the pump power is set to 10 mW, and the waveguide length is set to 8 mm in the calculation. (d) Photon flux intensity spectra of SFWM in the quasi-TE mode under different waveguide lengths. The pump wavelength is set to 1420 nm, the pump power is set to 10 mW, and the waveguide width is set to 450 nm in the calculation.

with a slightly reduced spectral width. It is obvious that the photon flux intensity spectra cannot cover the regions of C band and O band, showing that this commonly used strip waveguide cannot be used to achieve a cross-band quantum light source. It is worth noting that when the width of the strip waveguide changes, its dispersion characteristics would vary accordingly. Near-zero dispersion can be achieved near 1420 nm by reducing the width of the strip waveguide to ∼334 nm. However, the waveguide dispersion is very sensitive to variations in strip width, which highly enhances requirements for precise fabrication. Besides, propagation loss in the strip waveguide would also rise when its width is reduced, which is also unfavorable for this application.

The shallow-ridge silicon waveguide is also widely used in silicon photonic chips. Its quasi-TE mode has much lower propagation loss than that of the single-mode strip waveguide. The sketch of its cross-section is shown in Fig. 2(a). In the calculation, the height of the core is set to 220 nm and the height of the ridge is set to 70 nm. The width of the ridge is used as a structural parameter to control waveguide dispersion. The calculated waveguide dispersions of the waveguides with different ridge widths under different wavelengths are shown in Fig. 2(b). It can be seen that the dispersion curves of these shallow-ridge silicon waveguides are flat, with much smaller values than those of single-mode strip waveguides. Especially, the zero dispersion point is near 1420 nm for the waveguide with a ridge width of 550 nm, which is preferred to achieve broadband phase matching for SFWM, supporting broadband photon pair generation. The calculation results of photon flux intensity spectra of SFWM under different ridge widths are shown in Fig. 2(c). In this calculation, the pump wavelength is set to 1420 nm, the pump power is set to 10 mW, and the waveguide length is set to 8 mm. C band and O band are also indicated by light blue and green regions respectively. It can be seen that the shallow-ridge silicon waveguides can support broadband photon pair generation by SFWM thanks to their low dispersion from O band to C band. The widest spectrum is achieved in the waveguide with a ridge width of 550 nm. The zero dispersion point of this waveguide is 1420 nm, very close to the pump wavelength. The waveguide with a smaller ridge width has a higher maximum intensity since its mode field area is smaller, leading to a higher nonlinear coefficient. All the spectra shown in Fig. 2(c) cover both the C band and the O band, showing that the structural parameters of the shallow-ridge silicon waveguide have good tolerance for errors in fabrication. The photon flux intensity spectra of SFWM in the waveguide with a ridge width of 550 nm under different waveguide lengths are also calculated, and the results are shown in Fig. 2(d). Other parameters in the calculation are the same as those of Fig. 2(c). Compared with the single-mode strip waveguide, the shallow-ridge silicon waveguide has a larger mode field area, leading to a smaller nonlinear coefficient. It can be compensated by a longer waveguide length thanks to its property of low propagation loss. It can be seen that the shallow-ridge

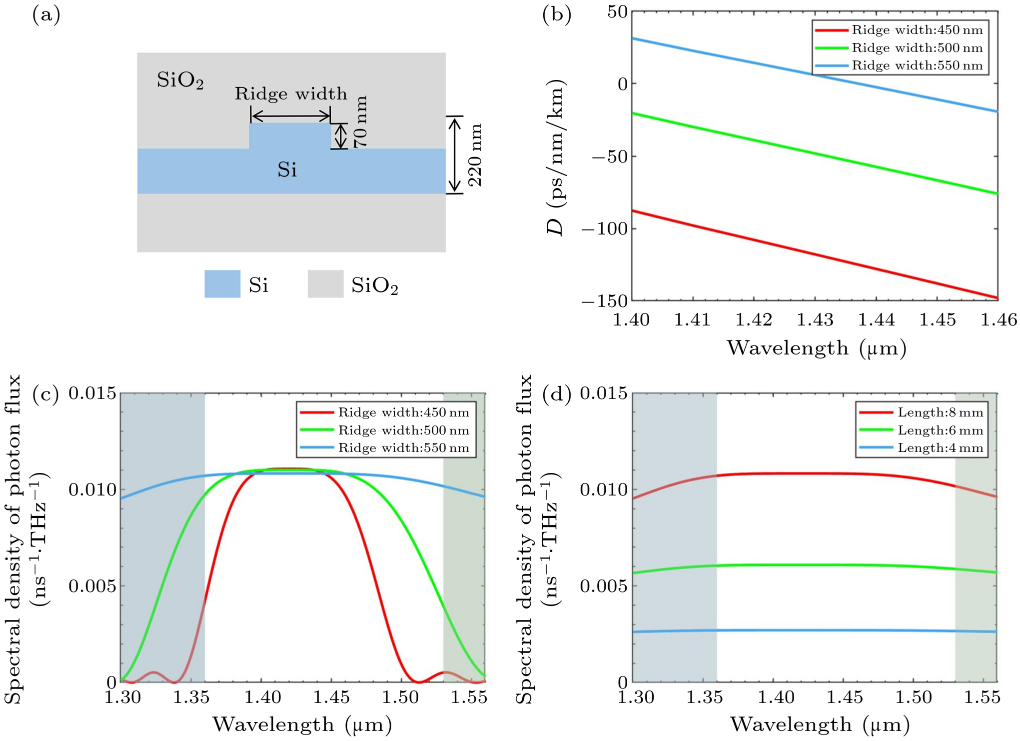

Fig. 2. Calculation results of shallow-ridge silicon waveguides. (a) The sketch of shallow-ridge silicon waveguide cross-section. (b) Dispersion curves of the quasi-TE mode of the waveguides with different ridge widths. (c) Photon flux intensity spectra of SFWM in the quasi-TE mode under different ridge widths. The pump wavelength is set to 1420 nm, the pump power is set to 10 mW, and the waveguide length is set to 8 mm in the calculation. (d) Photon flux intensity spectra of SFWM in the quasi-TE mode under different waveguide lengths. The pump wavelength is set to 1420 nm, the pump power is set to 10 mW, and the ridge width is set to 550 nm in the calculation.

waveguide with a length of 8 mm can achieve the same maximum intensity of the photon flux as that of a strip waveguide with a length of 6 mm. Although the bandwidth of the generated photon flux reduces slightly when the waveguide length increases, all the spectra can cover both the C band and O band. These results show that the shallow-ridge waveguide is a good candidate for achieving the proposed cross-band quantum light source based on SFWM. It is worth noting that the shallow etching process we used has an accuracy of 70 ± 5 nm. The impact of deviations in ridge height due to fabrication processes is also calculated. The results show that when the ridge height deviates by 5 nm, the waveguide has similar dispersion curves with a small deviation in the zero point (a few nanometers). The small variation in the dispersion curve would not lead to a large variation in the photon flux intensity spectrum of SFWM. Hence, deviations in ridge height due to fabrication processes would not significantly impact the performance of the proposed source.

Then, the impact of SpRS in silicon waveguides on such a cross-band quantum light source is investigated experimentally. SpRS is not a serious problem in silicon waveguide-based quantum light sources at the C band since the noise photons generated by SpRS in silicon waveguides are concentrated at some wavelengths far from the pump wavelength and can be simply removed by optical filters. However, in the cross-band quantum light source proposed in this work, the frequency shifts between the pump light and the generated signal and idler photons are over 15 THz. The impact of SpRS is not clear under this large frequency shift. Hence, we design an experiment to investigate the impact of SpRS; the setup is shown in Fig. 3(a). The waveguide used in this experiment is a piece of strip silicon waveguide with a core size of 450 nm $\times$ 220 nm and a waveguide length of 1.15 cm. To measure the noise photons generated by SpRS at different frequency shifts, a tunable laser system (Santec TSL-570) with a large tuning range (1355 nm–1640 nm) is used as the pump light source. The pump light at a specific wavelength (l_{p}) passes through a fiber polarization controller (FPC) and a band-stop filter system at C band; then it is coupled into the silicon waveguide, generating photons at C band through SpRS and SFWM in the silicon waveguide. The FPC is used to control the polarization state of the pump light, ensuring that it is coupled to the quasi-TE mode of the silicon waveguide. The band-stop filter system has cascaded dense wavelength division multiplexers (DWDMs), supporting a stop-band with a central wavelength (λ) at 1566.3 nm and a stop-band width of 0.8 nm. It removes the photons of the pump light and photons generated when the pump light propagates through the fibers beforehand, providing a clean wavelength window to measure the photons generated in the silicon waveguide. Then, the pump light and the generated photons are coupled out of the silicon waveguide and pass through a bandpass filter system with the same center wavelength as that of the band-stop one but narrower pass-band width, which is 0.2 nm. In this way, the generated photons in the

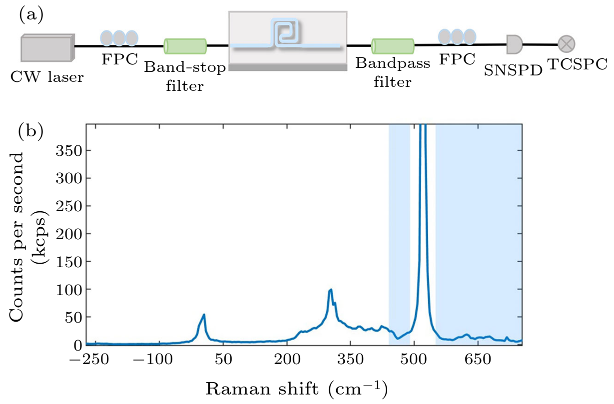

Fig. 3. Experiment of the impact of SpRS. (a) Sketch of the experimental setup. (b) Experimental result of the photons generated in a silicon waveguide under a weak pump level (1 mW). The blue regions show the frequency shifts can be used to design the wavelengths of the pump light and the signal/idler photons in the cross-band quantum light source.

waveguide at λ are selected and sent to a superconducting nanowire single-photon detector (SNSPD, PHOTEC, China) and recorded by a time-correlated single-photon counter (TCSPC, Swabian Instruments Time Tagger Ultra). Since the SNSPD is polarization-dependent, another FPC is used to control the polarization state of these photons to maximize their count rate.

In the experiment, the generated photons are measured under different pump wavelengths from 1400 nm to 1636 nm. The frequency shift of the generated photons, i.e., the frequency difference between the generated photons and the pump light, can be calculated according to λ (1566.3 nm) and the pump wavelength of each measurement. The pump power is set to a low level (1 mW), ensuring that SpRS is the main contribution to generating these photons. The measurement result is shown in Fig. 3(b). The horizontal axis uses "wavenumber (cm^{-1})" to represent the frequency shift of SpRS (denoted by $\Delta\nu$). It is defined as $\Delta\nu = 1/\lambda_{\mathrm{p}} - 1/\lambda_{\mathrm{R}}$, where λ_{p} and λ_{R} are the wavelengths of the pump light and SpRS photons in centimeters (cm), respectively. It can be seen that three peaks appear in the spectrum of the generated photons, which are located near frequency shifts of $0\,\mathrm{cm}^{-1}$, $300\,\mathrm{cm}^{-1}$, and $520\,\mathrm{cm}^{-1}$, respectively. According to the designs of the band-pass filter and band-stop filter, it can be confirmed that all of them contribute to SpRS. The peak at $520\,\mathrm{cm}^{-1}$ is the strongest one. The peak at $300\,\mathrm{cm}^{-1}$ is relatively weak with a flat floor. The SpRS photons in these two peaks would significantly impact the performance of the proposed cross-band quantum light source. Considering the large wavelength ranges of the C band (1530 nm–1565 nm) and O band (1260 nm–1360 nm), the frequency difference between the pump light and the signal/idler photons in the proposed cross-band quantum light source could be selected in the range of $460\,\mathrm{cm}^{-1}$–$770\,\mathrm{cm}^{-1}$. According to the result shown in Fig. 3(b), the region near $460\,\mathrm{cm}^{-1}$ between the two peaks and the region above the peak at $520\,\mathrm{cm}^{-1}$ can be used to design wavelengths for both pump light and signal/idler photons, which are indicated by blue regions in Fig. 3(b).

We designed and fabricated samples of shallow-ridge silicon waveguides to demonstrate the proposed cross-band quantum light source. They are fabricated on a silicon-on-insulator substrate with a top silicon layer of 200 nm in thickness. Three types of waveguides with different ridge widths are fabricated on the chip: 450 nm, 500 nm, and 550 nm, respectively. All the waveguides have the same ridge height and length, which are 70 nm and 8 mm, respectively. Edge couplers are designed at both ends of each waveguide; these are silica leaky ridge waveguide-based mode field converters supporting broadband optical coupling between waveguides and optical fibers. The measured insertion losses of these waveguides are about 4–5 dB at C band, mainly due to coupling losses. Since the mode field converters are optimized for C band, the insertion losses increase to 6–7 dB for light at the pump wavelength (near 1420 nm), and more than 8 dB for O-band photons.

The experimental setup for photon pair generation is shown in Fig. 4(a). The tunable laser system (Santec TSL-570) is used as the pump light source. The pump light at a specific wavelength (λ_{p}) is coupled to the quasi-TE mode of a shallow-ridge waveguide on the chip after it passes through an FPC for polarization adjustment and optical filters that remove noise photons at C band and O band. A 1310 nm/1450 nm wavelength division multiplexer (WDM) is used to remove noise photons from the pump light source in the range of 1260 nm–1360 nm. The pump light with a wavelength higher than 1390 nm can pass through it with a low loss of 0.4 dB. Then, a band-stop filter system similar to the one used in the setup for investigating SpRS [shown in Fig. 3(a)] is employed to provide a clean wavelength window at C band to measure the signal photons generated in the waveguide, with a central wavelength (λ_{s}) of 1538.2 nm, a width of 0.8 nm, and a loss of 0.9 dB. When the pump light propagates through the waveguide, broadband photon pairs are generated by SFWM. They are coupled out of the chip and pass through another 1310 nm/1450 nm WDM to separate signal photons at C band and idler photons at O band with losses of 0.28 dB and 0.12 dB, respectively. Then, the C-band photons pass through cascaded DWDMs to remove the pump light, and the signal photons at 1538.2 nm are selected with a loss of 3.5 dB. The O-band photons pass through cascaded 1310 nm/1450 nm WDMs with a loss of 0.9 dB to further remove the impact of the pump light; then an O-band tunable filter with a loss of 1.86 dB and a bandwidth of 1 nm is used to select idler photons at a specific wavelength (λ_{i}). Finally, the selected photons are detected by two SNSPDs (SNSPD, PHOTEC, China) and recorded by a TCSPC (Swabian Instruments Time Tagger Ultra). The SNSPD detecting C-band photons has an efficiency of 85% and a dark count rate of 400 Hz; while the one detecting O-band photons has an efficiency of 66% and a dark count rate of 200 Hz.

In this experimental setup, the wavelength of selected signal photons (λ_{s}) is fixed at 1538.2 nm, while the pump wavelength (λ_{p}) and the wavelength of selected idler photons (λ_{i}) can be adjusted. First, the two-photon coincidence measurements are carried out under the setting that

$\lambda_p = 1435.1\,\mathrm{nm}$ and $\lambda_i = 1345\,\mathrm{nm}$. The frequency difference between the pump light and the selected signal/idler photons is $466\,\mathrm{cm}^{-1}$, which is in the low noise region near $460\,\mathrm{cm}^{-1}$ shown in Fig. 3(b). Figure 4(b) shows the measured coincidence count rates and coincidence to accidental coincidence ratios (CARs) of the photons generated in the waveguide with a ridge width of 450 nm under different pump levels, indicated by the output power of the laser source. It shows that clear coincidence counts of detection events from two SNSPDs can be observed. The coincidence count rate rises and the CAR decreases with the increasing pump level. The time bin width used to calculate the CAR is 200 ps, covering the whole coincidence peak. The maximum CAR is ∼30, indicating clear cross-band photon pair generation. The measurement results of the photons generated in waveguides with ridge widths of 500 nm and 550 nm are shown in Figs. 4(c) and 4(d), respectively. The results are similar to those shown in Fig. 4(b), with maximum CARs of 33 and 42, respectively. These results show that all three waveguides support cross-band photon pair generation in this wavelength setting. The waveguide with a ridge width of 550 nm has the best performance, which agrees with the theoretical results shown in Fig. 2(d).

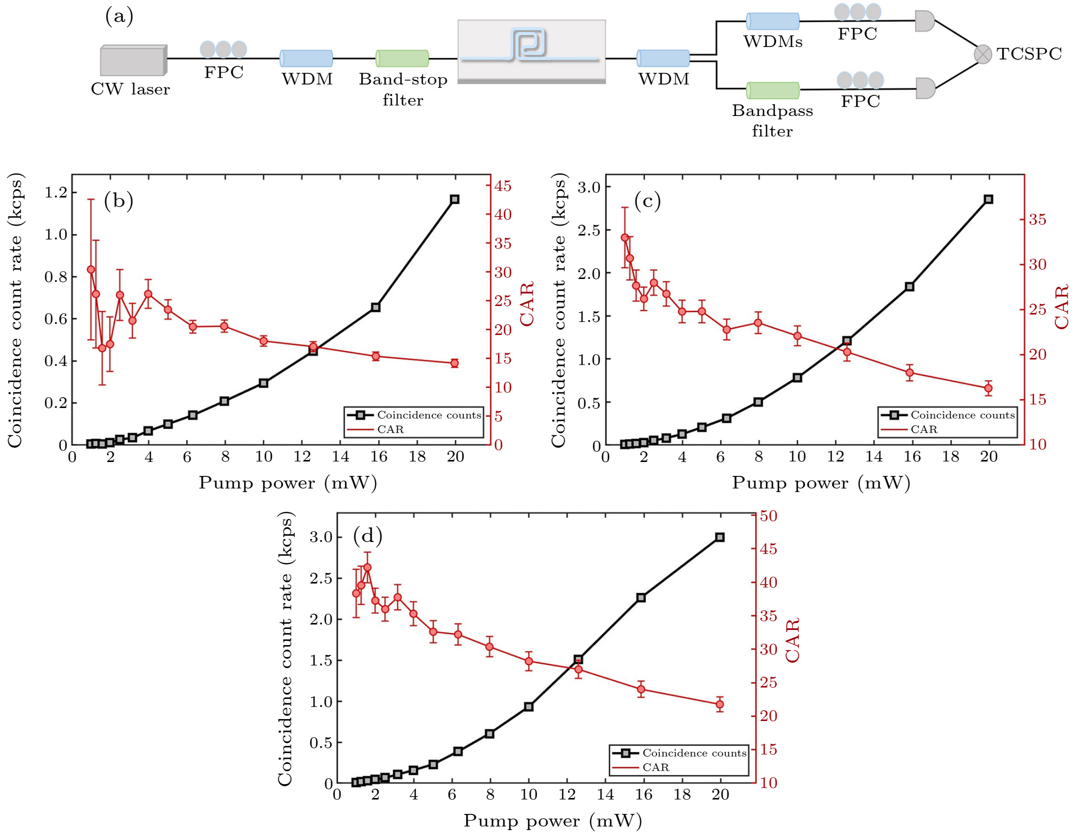

Fig. 4. Photon pair generation by SFWM in shallow-ridge silicon waveguide under the wavelength settings that $\lambda_p = 1435.1\,\mathrm{nm}$, $\lambda_s = 1538.2\,\mathrm{nm}$, and $\lambda_i = 1345\,\mathrm{nm}$. (a) Sketch of the experimental setup. (b)–(d) The coincidence count rates and CARs of the photons generated in the waveguides with ridge widths of 450 nm, 500 nm, and 550 nm, respectively.

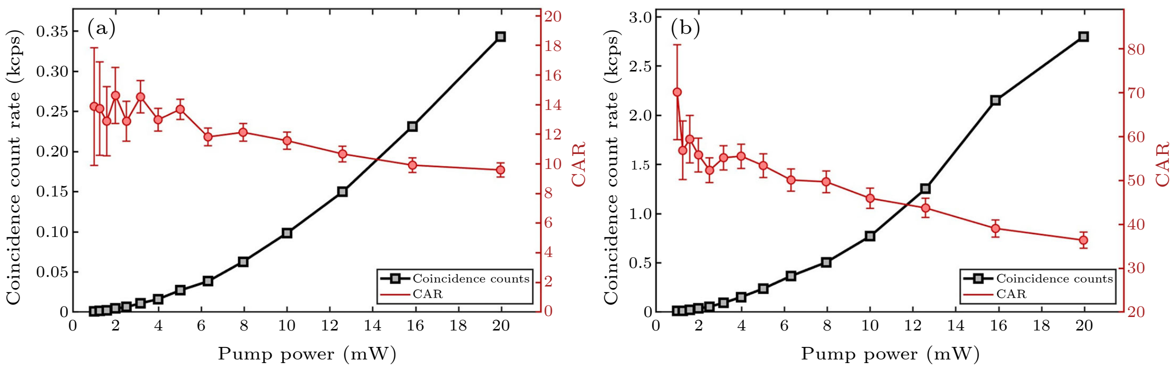

Fig. 5. Photon pair generation by SFWM in shallow-ridge silicon waveguide under the wavelength settings that $\lambda_p = 1409.1\,\mathrm{nm}$, $\lambda_s = 1538.2\,\mathrm{nm}$, and $\lambda_i = 1300\,\mathrm{nm}$. (a) and (b) The coincidence count rates and CARs of the photons generated in the waveguides with ridge widths of 500 nm and 550 nm, respectively.

The two-photon coincidence measurements are also carried out under the settings that $\lambda_p = 1409.1\,\mathrm{nm}$ and $\lambda_i = 1300\,\mathrm{nm}$. In these settings, the frequency difference between the pump light and the selected signal/idler photons is $596\,\mathrm{cm}^{-1}$, which is in the low noise region above $520\,\mathrm{cm}^{-1}$. It shows that no obvious coincidence counts can be observed in the experiment using the waveguide with a ridge width of 450 nm. The measurement results of the coincidence rates and CARs using waveguides with ridge widths of 500 nm and 550 nm are shown in Figs. 5(a) and 5(b), respectively. It can be seen that in the experiment with the waveguide having a ridge width of 550 nm, the result of coincidence count rate is similar to that shown in Fig. 4(d). While a higher CAR is achieved, indicating a smaller impact of SpRS under a larger frequency difference between the pump light and signal/idler photons. On the other hand, in the experiment with the waveguide having a ridge width of 500 nm, both coincidence count rates and CARs are much lower than those shown in Fig. 4(c). These results show that shallow-ridge silicon waveguides with a ridge width of 550 nm are preferred for achieving cross-band quantum light sources thanks to their optimized waveguide dispersion supporting wider bandwidth for photon pair generation by SFWM.

The above experiments demonstrate the feasibility of cross-band quantum light sources based on SFWM in shallow-ridge silicon waveguides. It is worth noting that the coupling loss between the waveguide and fiber at O band is quite high in the sample chip since the mode field converters at the ends of waveguides are optimized for C band. Broadband mode field converters covering both C band and O band are preferred for this application. Besides, the filter bandwidths of the selected C-band and O-band photons differ in the experiments. It can be expected that the performance of photon pair generation could be further improved by better filter band matching.

In summary, a cross-band quantum light source is proposed in this work. It generates photon pairs where one photon in a pair is at C band and the other is at O band. This source is based on SFWM in a piece of shallow-ridge silicon waveguide. By adjusting the ridge width, the waveguide dispersion of the shallow-ridge silicon waveguide is optimized to achieve ultra-broadband photon pair generation. The SpRS in silicon waveguides is investigated experimentally. It shows that there are two regions in the spectrum of generated photons from SpRS, which could be used to achieve cross-band photon pair generation. A chip of waveguide samples with different ridge widths is fabricated, by which cross-band photon pair generation is demonstrated experimentally. The experimental results show that the source can be achieved using dispersion-optimized shallow-ridge silicon waveguides. This quantum light source provides a way to develop new fiber-based quantum communication applications utilizing both C band and O band, which helps fully utilize resources of optical fiber networks.

Acknowledgements. This work was supported by the Quantum Science and Technology-National Science and Technology Major Project (Grant No. 2024ZD0302502 for WZ), the National Natural Science Foundation of China (Grant No. 92365210 for WZ), Tsinghua Initiative Scientific Research Program (for WZ), and the project of Tsinghua University-Zhuhai Huafa Industrial Share Company Joint Institute for Architecture Optoelectronic Technologies (JIAOT, for YH).

References

[1] Lu X, Li Q, Westly D A *et al.* 2019 *Nat. Phys.* **15** 373
[2] Wengerowsky S, Joshi S K, Steinlechner F *et al.* 2018 *Nature* **564** 225
[3] Wei K J, Hu X, Du Y Q *et al.* 2023 *Photonics Res.* **11** 1364
[4] Du Y Q, Zhu X, Hua X *et al.* 2023 *Chip* **2** 100039
[5] Sibson P, Erven C, Godfrey M *et al.* 2017 *Nat. Commun.* **8** 13984
[6] Tang Y L, Yin H L, Chen S J *et al.* 2014 *Phys. Rev. Lett.* **113** 190501
[7] Du Y, Li B H, and Hua X 2025 *Light Sci. Appl.* **14** 108
[8] Paesani S, Ding Y, Santagati R *et al.* 2019 *Nat. Phys.* **15** 925
[9] Madsen L S, Laudenbach F, Askarani M F *et al.* 2022 *Nature* **606** 75
[10] Llewellyn D, Ding Y, Faruque I I *et al.* 2020 *Nat. Phys.* **16** 148
[11] Tanzilli S, De Riedmatten H, Tittel W *et al.* 2001 *Electron. Lett.* **37** 26
[12] Tanzilli S, Tittel W, De Riedmatten H *et al.* 2002 *Eur. Phys. J. D* **18** 155
[13] Nosaka T, Das B K, Fujimura M *et al.* 2006 *IEEE Photonic. Tech. L.* **18** 124
[14] Wang C, Langrock C, Marandi A *et al.* 2018 *Optica* **5** 1438
[15] Domeneguetti R, Stefszky M, Herrmann H *et al.* 2023 *Opt. Lett.* **48** 2999
[16] Shi X, Mohanraj S S, Dhyani V *et al.* 2024 *Light Sci. Appl.* **13** 282
[17] Takesue H and Inoue K 2005 *Opt. Express* **13** 7832
[18] Cheng J R, Zhang W, Zhou Q *et al.* 2010 *Chin. Phys. Lett.* **27** 124208
[19] Feng L T, Cheng Y J, Qi X Z *et al.* 2023 *Optica* **10** 702
[20] Ma C X, Wang X X, Anant V *et al.* 2017 *Opt. Express* **25** 32995
[21] Paesani S, Borghi M, Signorini S *et al.* 2020 *Nat. Commun.* **11** 2505
[22] Kues M, Reimer C, Roztocki P *et al.* 2017 *Nature* **546** 622
[23] Liu J Y, Liu D N, Jin Z P *et al.* 2024 *Sci. Adv.* **10** eado9822
[24] Liu M T and Lim H C 2013 *Opt. Express* **21** 30358
[25] Cordier M, Delaye P, Gérôme F *et al.* 2020 *Sci. Rep.* **10** 1650
[26] Wang Z, Liu H, Sun Q *et al.* 2014 *Opt. Express* **22** 31486
[27] Jin B, Yuan J, Yu C *et al.* 2014 *Opt. Express* **22** 6257
[28] Driscoll J B, Ophir N, Grote R R *et al.* 2012 *Opt. Express* **20** 9227
[29] Zhu M, Liu H J, Li X F *et al.* 2012 *Opt. Express* **20** 15899
[30] Liu Q, Gao S, Li Z *et al.* 2011 *Appl. Opt.* **9** 1260
[31] Kues M, Reimer C, Lukens J M *et al.* 2019 *Nat. Photon.* **13** 170
[32] Koefoed J G, Müller R R, and Rottwitt K 2023 *IEEE J. Sel. Top. Quantum Electron.* **29** 6700207
[33] Brainis E 2009 *Phys. Rev. A* **79** 023840